



# Effect of annealing time on the microstructure, crystal quality and optoelectronic properties of Er-Ga<sub>2</sub>O<sub>3</sub> films

Zi Wang<sup>1</sup>, Zhuoxuan Zhang<sup>1</sup>, Xiaokun Yang<sup>1,\*</sup>, Jie Liu<sup>2</sup>, and Hongdi Xiao<sup>2</sup>

<sup>1</sup>School of Physics and Electronics, Hunan University, Changsha 410082, China

<sup>2</sup>School of Microelectronics, Shandong University, Jinan 250100, China

Received: 15 November 2022

Accepted: 10 February 2023

Published online:

6 April 2023

© The Author(s), under exclusive licence to Springer Science+Business Media, LLC, part of Springer Nature 2023

## ABSTRACT

The post-annealing process is an effective method to improve the properties of gallium oxide (Ga<sub>2</sub>O<sub>3</sub>) single crystal films. However, the studies on post-annealing of Ga<sub>2</sub>O<sub>3</sub> films have been largely limited to the annealing temperature, with few reports of the annealing time. Here, we show the effect of annealing time on the Er-doped β-Ga<sub>2</sub>O<sub>3</sub> (−201) epitaxial films deposited by pulsed laser deposition. The Ga<sub>2</sub>O<sub>3</sub> film with a bandgap of ~ 4.98 eV and annealed at 900 °C for 15 min, exhibits the best crystal quality and optical property in comparison with the films before and after the annealing for 7 and 30 min in air. The epitaxial relationship between the film and substrate is Ga<sub>2</sub>O<sub>3</sub> [010] || GaN [−12−10] with Ga<sub>2</sub>O<sub>3</sub> (−201) || GaN (0001). Moreover, the resistivity of the 15 min-annealed Ga<sub>2</sub>O<sub>3</sub> film, which is about 180 Ω·cm, still maintains a low level.

## 1 Introduction

Gallium oxide (Ga<sub>2</sub>O<sub>3</sub>) has shown great potential in optoelectronics and power electronics due to its excellent properties such as the wide band gap of ~ 4.9 eV, high breakdown electric field of 8 MV/cm, and high Baliga's Figure of Merit of 3444 [1–7]. In particular, the epitaxial β-Ga<sub>2</sub>O<sub>3</sub> films, as an ideal host material for rare earth (RE-) dopants, have been successfully used to fabricate Ga<sub>2</sub>O<sub>3</sub>-based LEDs [8, 9]. These Ga<sub>2</sub>O<sub>3</sub>-based LEDs have drawn huge attention for their low drive voltage, long service life, and stable light output [10, 11]. However, with the weak luminous efficiency, the application of Ga<sub>2</sub>O<sub>3</sub>-

based LEDs has been limited. To the best of our knowledge, the key to fabricating high-performance devices lies in the quality of Ga<sub>2</sub>O<sub>3</sub> films [12, 13]. This is where we are devoting our efforts.

For RE-doped Ga<sub>2</sub>O<sub>3</sub> films, in addition to optimizing the deposition conditions, the post-annealing process is an effective method to improve the crystal quality and optoelectronic properties. In our previous study, the single crystal Er-doped Ga<sub>2</sub>O<sub>3</sub> (Er-Ga<sub>2</sub>O<sub>3</sub>) film, which could be used to fabricate LEDs with a low voltage-driven green emission [10], has been successfully deposited on the etched nanoporous (NP) GaN substrates via pulsed laser deposition (PLD) [14]. Furthermore, we find that the crystalline quality and photoluminescence efficiency of Ga<sub>2</sub>O<sub>3</sub>

Address correspondence to E-mail: xkyang@hnu.edu.cn

films could be improved significantly after annealing at 900 °C in comparison with other annealing temperatures [8]. Notably, the annealing time is an important factor for the recrystallization process on many semiconductors and metals oxide, such as ZnO, NiO, FeO, CuO, CoO, etc[15–22], and its effect cannot be neglected. However, research on the annealing time of Ga<sub>2</sub>O<sub>3</sub> films has been rarely reported, which is the aim of this work.

In this work, NP GaN wafers with a porosity of 40% were obtained by electrochemical (EC) etching, and then the Er-Ga<sub>2</sub>O<sub>3</sub> films were deposited on the NP-GaN wafers by PLD. After deposition, the Ga<sub>2</sub>O<sub>3</sub> films were annealed at 900 °C for 7, 15 and 30 min in air, respectively. The microstructure, crystal quality and optoelectronic properties of the films show a remarkable correlation with the annealing time. In comparison to the samples before and after annealing for 7 and 30 min, the Er-doped Ga<sub>2</sub>O<sub>3</sub> film annealing for 15 min exhibits the best crystal quality and optical properties. Furthermore, the resistivity of the 15 min-annealed Ga<sub>2</sub>O<sub>3</sub> film is only ~ 180 Ω cm.

## 2 Experimental

Firstly, the n-GaN wafers were transformed into NP-GaN by the EC etching [23], and the detail of EC etching for n-GaN was provided in supplementary materials (Fig. S1). Subsequently, the NP-GaN with a porosity of 40% was used to deposit Er-Ga<sub>2</sub>O<sub>3</sub> films by PLD system. The wavelength of the KrF laser is 248 nm, and the laser power was ~ 6 J/cm<sup>2</sup> with a frequency of 2 Hz. The pressure of the reactor chamber was 0.09 Pa in N<sub>2</sub> condition with a flow of 25 sccm. The distance between the substrates and Ga<sub>2</sub>O<sub>3</sub> pellet targets (with 2.5 at% erbium oxide) was about 100 mm. The substrates were heated to 700 °C, and the PLD experiment lasted 60 min. After deposition, the Er-Ga<sub>2</sub>O<sub>3</sub> films were annealed at 900 °C for 7, 15 and 30 min in air, respectively.

The morphologies of Er-Ga<sub>2</sub>O<sub>3</sub> films were measured using Scanning electron microscope (SEM, Helios G4 UC). The crystal quality and epitaxial relationship were analyzed via High-resolution X-ray diffractometer (HRXRD, Smartlab3kW). The chemical composition studies were carried out via X-ray photoelectron spectroscopy (XPS, ESCALAB MK II). The X-ray source was Al Kα (hν = 1486.6 eV), electron emission angle was 58°, and the base pressure was

8 × 10<sup>-10</sup> Pa. The size of the analyzed sample area was 500 μm in diameter. Before the XPS measurement, the sample was not sputter-etched by using Ar<sup>+</sup>, the charge neutralizer was used. A high-resolution transmission electron microscope (HRTEM, JEM-2100) with Tecnai F30 transmission electron microscope was employed to investigate the atomic arrangements and selected area electron diffraction (SAED). Photoluminescence (PL) spectra were obtained using a confocal Raman imaging system (Renishaw inVia-Reflex Raman Microscope), 532 nm laser with 1800 lines mm<sup>-1</sup> grating is used. The wavelength range is 540–560 nm, and the laser power is 10 mW, the integration time is 5s.

## 3 Results and discussion

Figure 1a shows the XRD spectra of Er-Ga<sub>2</sub>O<sub>3</sub> films deposited on NP-GaN before and after annealing at 900 °C for 7, 15 and 30 min, respectively. In addition to the peaks related to sapphire and GaN, three peaks located at ~ 18.8, ~ 38.3 and ~ 59.0° were clearly observed, corresponding to the (–201), (–402) and (–603) diffraction planes of β-Ga<sub>2</sub>O<sub>3</sub> (JCPDS NO.43-1012), respectively. This implies that the films are β-Ga<sub>2</sub>O<sub>3</sub> growing along the [–201] direction. The full width at half maximum (FWHM) of the (–201) peaks is ~ 0.501, ~ 0.462, ~ 0.311 and ~ 0.443°, respectively, indicating that the 15 min-annealed Ga<sub>2</sub>O<sub>3</sub> film exhibits the best crystal quality. The rocking curve of (–201) peak presents good symmetry with an FWHM of ~ 1.41°, implying the excellent crystal quality of 15 min-annealed Er-Ga<sub>2</sub>O<sub>3</sub> film (Fig. 1b). This indicates that the re-crystallization process cannot complete as the annealing time is not enough. On the contrary, the crystal lattice structure could be damaged (lattice distortion increase) due to the extra energy (thermal energy) after complete recrystallization (> 15 min). This could be attributed to the difference of the thermal expansion coefficient between the GaN substrate and Ga<sub>2</sub>O<sub>3</sub> film [24, 25]. Moreover, we find the (–201) peaks slightly shift to a large angle with increasing the annealing time, as shown in Fig. 1c. The shift is due to the decrease in grain size of the films or the increase in stress between the films and the substrates [26]. The β-Ga<sub>2</sub>O<sub>3</sub> grown on GaN has a large tensile stress [14], thus the shift suggests that internal stress of the film is released.

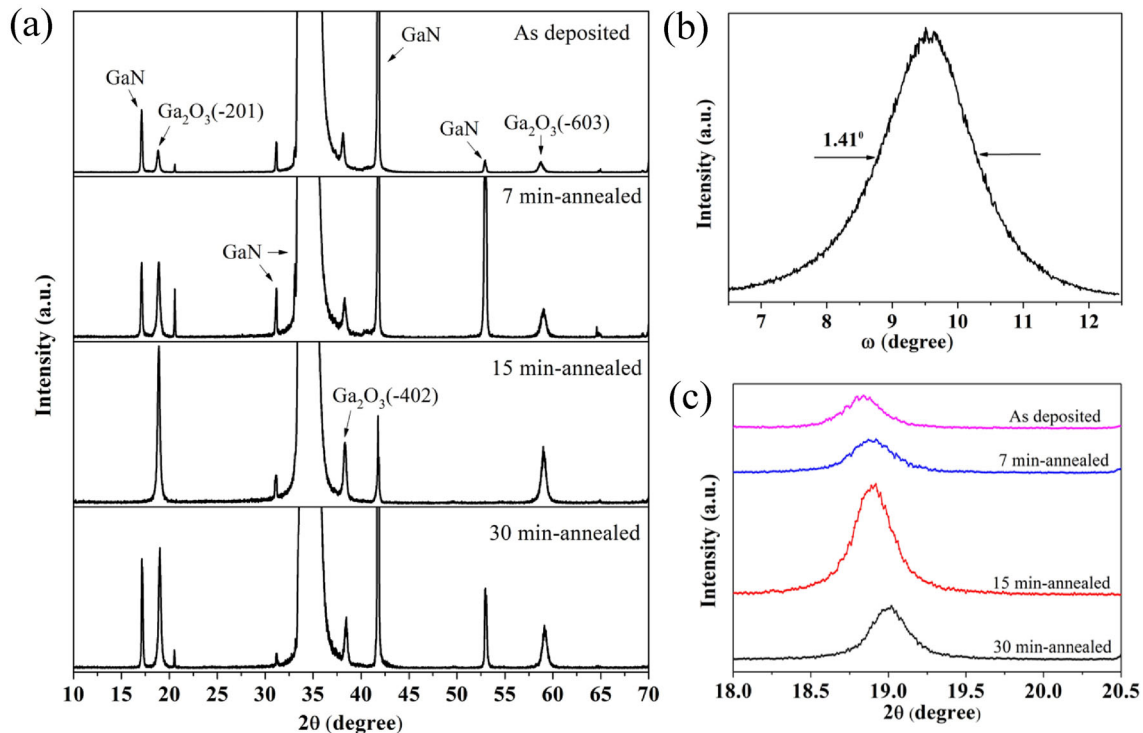


**Fig. 1** **a** XRD spectra of the Er-Ga<sub>2</sub>O<sub>3</sub> films on the NP-GaN before and after the annealing at different time: as-deposited, 7 min, 15 and 30 min; **b** rocking curve of 15 min-annealed Er-Ga<sub>2</sub>O<sub>3</sub> film (-201) peak, and **c** magnified XRD spectra of the (-201) peak

SEM was performed to further investigate the change in the grain size of the films. Figure 2 shows the top-view SEM images of the Er-doped Ga<sub>2</sub>O<sub>3</sub> films before and after annealing at 900 °C for 7, 15 and 30 min, respectively. The Er-Ga<sub>2</sub>O<sub>3</sub> film before annealing consists of irregular-shaped grains, and the blurred boundaries of the grains led to the large crystal grain size (100 nm in diameter), as shown in Fig. 2a. However, the regular-shaped grains with well-defined boundaries are observed at the surface of the annealed films, due to the recrystallization phenomenon caused by high temperature annealing [27–31]. The average grain sizes of the films after annealing for 7, 15 and 30 min are ~ 85, ~ 60 and ~ 40 nm, respectively. According to Fig. 1c, the decrease in grain size of the films resulted in XRD peaks slightly shift to large angle. This result demonstrates that the annealing process could affect the microstructures of the films. More specifically, both the grain size and the density decreased with increasing the annealing time. In the meanwhile, boundaries shape. The regular and dense grains lead to the best crystal quality for 15 min-annealed Er-Ga<sub>2</sub>O<sub>3</sub> film [32]. The following discussion will focus

on the epitaxial relationship and stoichiometry of the 15 min-annealed Er-Ga<sub>2</sub>O<sub>3</sub> film.

The out-of-plane epitaxial relationship between the 15 min-annealed films and the substrate was evaluated using TEM. Figure 3a depicts the cross-sectional HRTEM image of the 15 min-annealed film. The crystal lattice of the film is arranged orderly and clearly, and the spacing of the interplane for the film is 0.471 nm, indicating the out-of-plane epitaxial relationship between the substrate and the film is GaN (0001) || Ga<sub>2</sub>O<sub>3</sub> (-201) [8, 33]. SAED pattern of the interface area between the GaN and the film are displayed in Fig. 3b. The diffraction dots of GaN (111), (110), and (0001) as well as β-Ga<sub>2</sub>O<sub>3</sub> (222), (800), (400), and (-201), which were deduced via the interplanar spacing and angles, were marked by white arrows, and further prove the out-of-plane epitaxial relationship for GaN (0001) || Ga<sub>2</sub>O<sub>3</sub> (-201). Figure 3c depicts the low-magnification TEM graph. The thickness of 15-min annealed film is 80 nm, and the diameter of the crystal grain along the film surface is 60 nm, which is consistent with the SEM results.

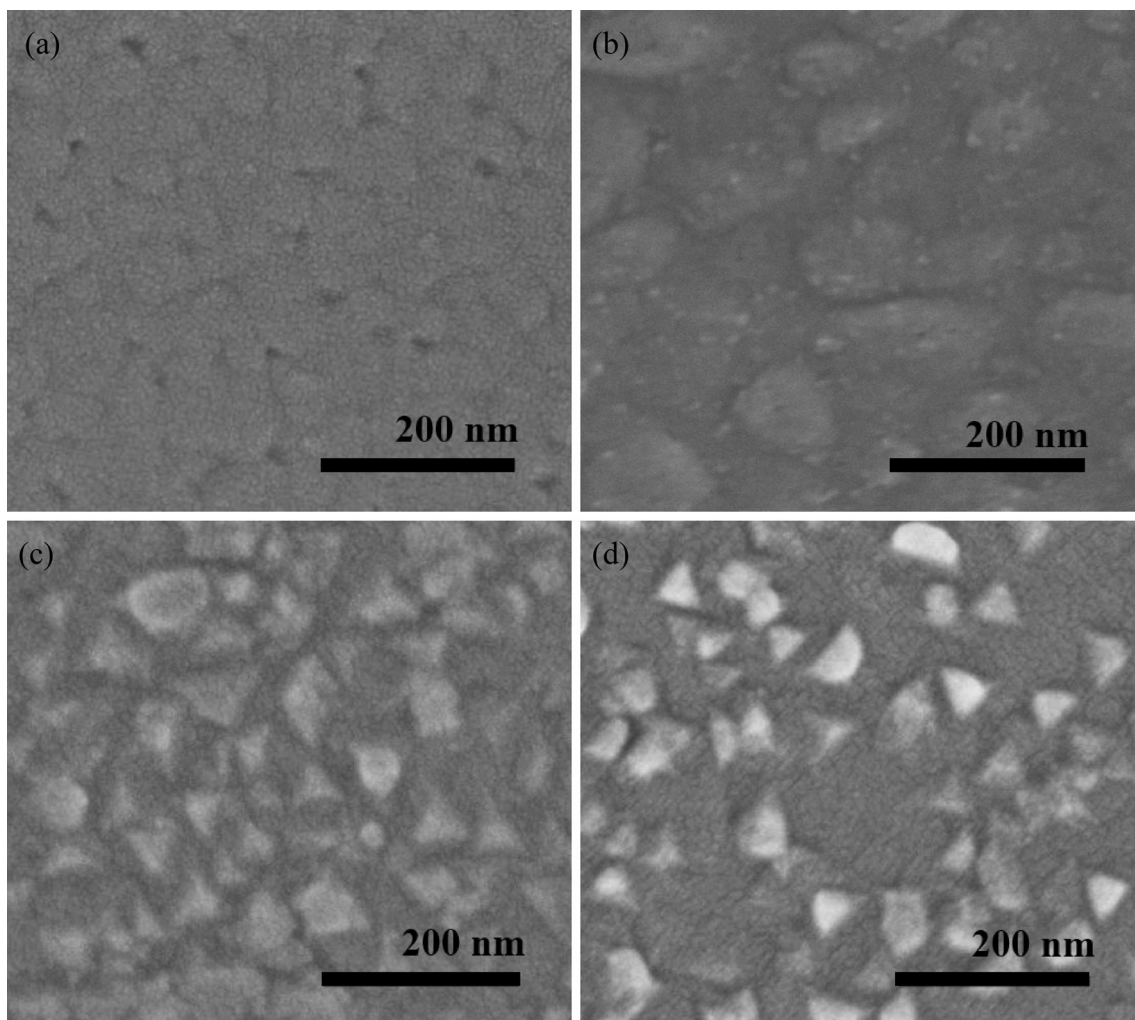


**Fig. 2** Top-view SEM images of the Er-Ga<sub>2</sub>O<sub>3</sub> films before and after the annealing at different time: **a** as-deposited, **b** 7 min, **c** 15 min and **d** 30 min

The  $\Phi$  scan XRD of Ga<sub>2</sub>O<sub>3</sub> {−401} and GaN {10–12} planes were employed to study the in-plane relationship, as shown in Fig. 4. The inclination angles of the GaN {10–12} and the Ga<sub>2</sub>O<sub>3</sub> {−401} are 39.01° and 23.44°. Six peaks separated by 60° were observed for GaN {10–12} plane as well as Ga<sub>2</sub>O<sub>3</sub> {−401} plane, exhibiting the six-fold symmetry of GaN {10–12} planes along GaN [0001]. For  $\beta$ -Ga<sub>2</sub>O<sub>3</sub>, however, the {401} planes are twofold in-plane rotation symmetry and therefore the 15 min-annealed film is tripartite domain structure. In addition, the coincident diffraction peaks of the GaN and Ga<sub>2</sub>O<sub>3</sub> demonstrate that the in-plane epitaxial relationship between the substrate and the film is GaN [−12−10]||Ga<sub>2</sub>O<sub>3</sub> [010]. The result is in agreement with our previous researches [8, 14].

The stoichiometry and element composition of the Er-Ga<sub>2</sub>O<sub>3</sub> films were investigated via XPS measurements, as shown in Fig. 5 and Fig. S2–4. For all samples, Ga2p, Ga3d, Ga LMM, O1s and O KILL Auger peaks are detected, as shown in the survey spectra. The binding energy was calibrated with the adventitious C1s peak via Eq. 289.58 -  $\phi_{SA}$  [34], where  $\phi_{SA}$  is the work function of Ga<sub>2</sub>O<sub>3</sub> (4.72 eV) [35]. Herein, the value of C1s peak is calculated to be 284.96 eV (cf. Figure 5b, Fig. S2b, S3b and S4b). The Ga 2p<sub>3/2</sub> and Ga 2p<sub>1/2</sub> peaks are centered at 1145.4 and 1118.5 eV ( $\Delta = 26.9$  eV) (cf. Figure 5c, Fig. S2c, S3c and S4c), as expected for the Ga<sup>3+</sup> oxidation state (stoichiometric Ga<sub>2</sub>O<sub>3</sub>) [36, 37]. For O1s peaks, only one single peak located at 530.7 eV is observed, corresponding to the Ga–O bonding in the film [38]. The atomic ratio of Ga to O is 72.5%, 70.7%, 69.8% and 69.3% for 0, 7, 15 and

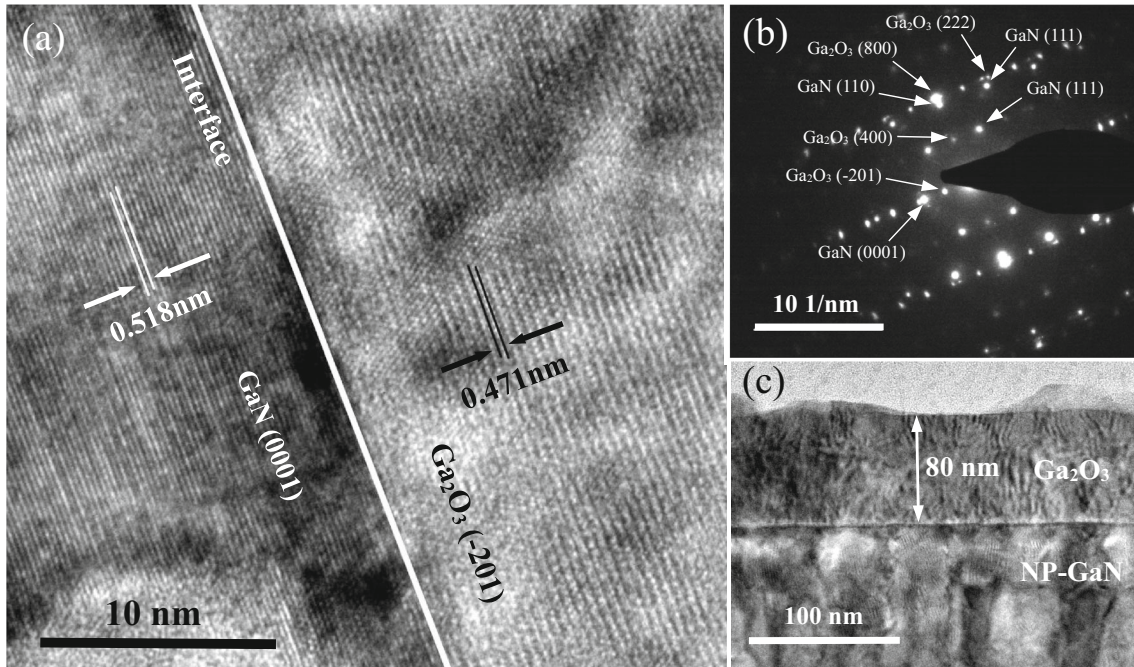


**Fig. 3** a HRTEM, b SEAD pattern and c low magnification TEM images of the interface between the 15 min-annealed film and NP-GaN.

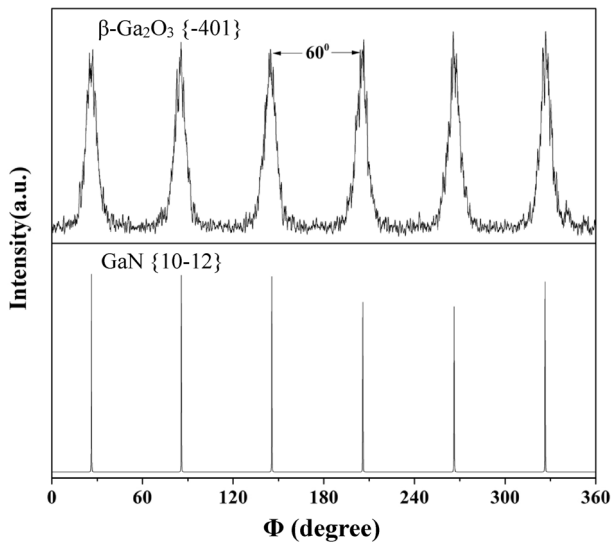


**Fig. 4**  $\Phi$  scan of GaN {10–12} planes for NP-GaN (0001) substrate and  $\text{Ga}_2\text{O}_3$  {–401} planes for 15 min-annealed Er- $\text{Ga}_2\text{O}_3$  (–201) plane

30 min-annealed films respectively, calculated by atomic sensitivity factor method (supplementary material). This suggests the decrease in oxygen vacancy of the film during the post-annealing and either a Ga-rich growth mode or the presence of oxygen vacancies near the surface [37]. Furthermore, the band gap of the films could be deduced by the energy-loss spectrum of O1s [39, 40]. The maximum

negative slope segment was linearly extrapolated to the datum, and then the energy band gap of  $\sim 4.88$ ,  $\sim 4.94$ ,  $\sim 4.98$  and  $\sim 5.02$  eV could be determined via the cross-point, as shown in the inset of Fig. 5 and Fig. S2-4 [41, 42]. The increase of the band gap is due to the decrease in oxygen vacancy of the film [43, 44].

The effect of the annealing time on the optical properties of the  $\text{Ga}_2\text{O}_3$  films were studied via PL spectra, as shown in Fig. 6a. The strongest emission peaks located at 548 nm, corresponding to the transition of  $^4\text{S}_{3/2} \rightarrow ^4\text{I}_{5/2}$  of Er- $\text{Ga}_2\text{O}_3$ , were observed in all films [45, 46]. However, the satellite peaks centered at 553 nm are attributed to Stark splitting caused by the spin-orbit splitting of the energy level. In Fig. 1, we observe that the PL intensities of the films are associated with the crystal quality. Thanks to its superior crystal structure, the 15 min-annealed film presents the highest PL intensity. This is the consequence of the reduction of defects, which capture the photocarriers and thus degrade PL intensity. Similar phenomenon has also been discovered in our previous studies [14].

Based on the above, the post-annealing process could improve the properties of  $\text{Ga}_2\text{O}_3$  single crystal films. However, the resistivity of the film, an important factor for electronics application, could degrade

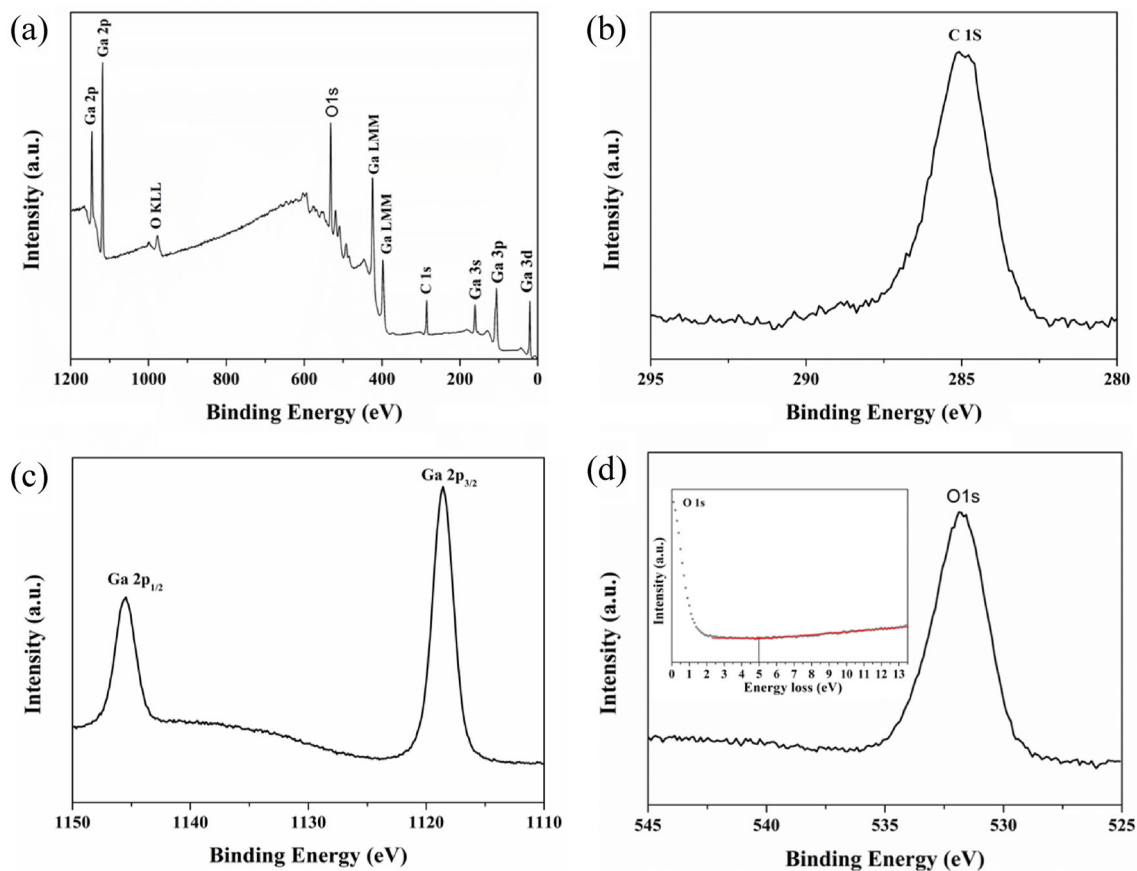


**Fig. 5** XPS spectra of the Er-Ga<sub>2</sub>O<sub>3</sub> film after 15 min annealed: **a** survey, **b** C 1s, **c** Ga 2p and **d** O 1s. The inset is O 1s energy-loss spectra to deduced the band gap of the film

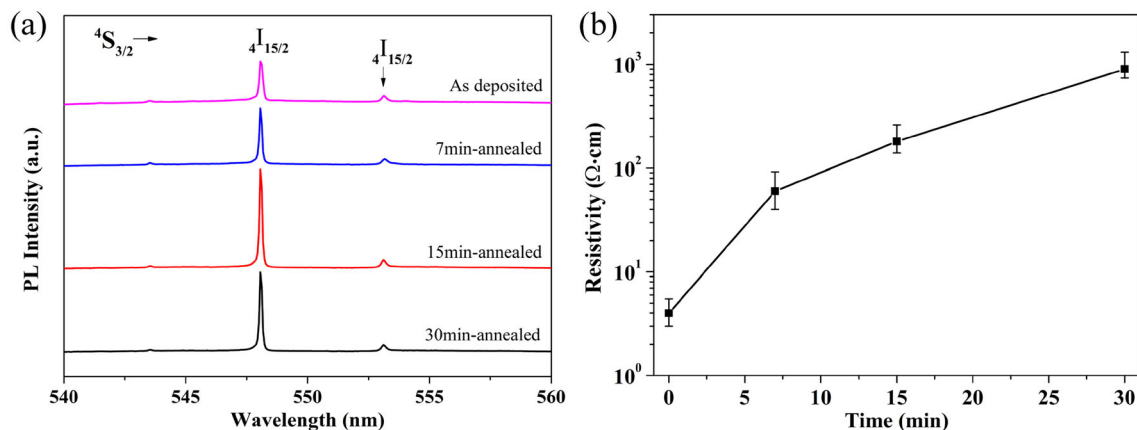


**Fig. 6** **a** PL spectra and **b** resistivity of the Er-Ga<sub>2</sub>O<sub>3</sub> before and after the annealing at different time.

with the decrease in oxygen vacancy of the film during the post-annealing [8, 47, 48]. Figure 6b displays the difference of the resistivity of Ga<sub>2</sub>O<sub>3</sub> film before and after annealing. The resistivity of the film form  $\sim 4 \text{ } \Omega \text{ cm}$  increase to  $\sim 900 \text{ } \Omega \text{ cm}$  with increasing the annealing time up to 30 min. Enough

annealing time benefits in decreasing the oxygen vacancy which plays a major role in conductivity, in line with the XPS results. The resistivity of 15 min-annealed film is only  $\sim 180 \text{ } \Omega \text{ cm}$ , remaining an excellent level for optoelectronics application.

## 4 Conclusion

In conclusion, the Er-Ga<sub>2</sub>O<sub>3</sub> films deposited on NP-GaN substrates were annealed at 900 °C with different annealing time. The effect of the annealing time on Er doped Ga<sub>2</sub>O<sub>3</sub> films was studied. The microstructure, crystal quality and optoelectronic properties of the films show a remarkable correlation with the annealing time. The recrystallization process cannot complete if the annealing time less than 15 min. On the contrary, the crystal lattice structure could be damaged due to the extra energy after complete recrystallization (> 15 min). SEM images, magnified XRD results demonstrate the crystal grain size decreased, density decreased and boundaries shaped as the annealing time increased. XPS results imply that the band gap increased as the annealing time increased, which should be attributed to the decrease in oxygen vacancy of the film. The PL intensities of the films are positively associated with the crystal quality (depend on the annealing time), and the 15 min-annealed film with the best crystal quality presents the highest PL intensity. The resistivity of the films increased as the annealing time increased, this is due to the decrease in oxygen vacancy (play an major role in conductivity) of the film during the post-annealing. Furthermore, the epitaxial relationship between the substrate and film is GaN [-12-10] || Ga<sub>2</sub>O<sub>3</sub> [010] with GaN (0001) || Ga<sub>2</sub>O<sub>3</sub> (-201). Limiting the annealing time to 15 min, the resistivity of Ga<sub>2</sub>O<sub>3</sub> film could keep up a low level (~ 180 Ω cm).

## Author contributions

ZW: conceptualization, methodology, investigation, writing-original draft, data curation. ZZ: conceptualization, project administration, validation, writing - review & editing. XY: conceptualization, supervision, resources. JL: software, validation. HX: supervision, writing - review & editing, funding acquisition.

## Funding

This work is supported by the National Natural Science Foundation of China (61874067).

## Data availability

The data supporting the conclusions of this article are included within the article.

## Declarations

**Conflict of interest** The authors declare that they have no known competing financial interests or personal relationships that could have appeared to influence the work reported in this paper.

**Supplementary Information:** The online version contains supplementary material available at <http://doi.org/10.1007/s10854-023-10371-4>.

## References

1. C. Zhou, Q. Ai, X. Chen, X. Gao, K. Liu, D. Shen, *Chin. Phys. B* **28**, 048503 (2019)
2. M. Hegde, I.D. Hosein, P.V. Radovanovic, *J. Phys. Chem. C* **119**, 17450–17457 (2015)
3. T. Miyata, T. Nakatani, T. Minami, *J. Lumin.* **87**, 1183–1185 (2000)
4. J. Hao, Z. Lou, I. Renaud, M. Cocivera, *Thin Solid Films* **467**, 182–185 (2004)
5. Y. Liu, L. Du, G. Liang, W. Mu, Z. Jia, M. Xu, Q. Xin, X. Tao, A. Song, *IEEE Electron. Dev. Lett.* **39**, 1696–1699 (2018)
6. S. Yu, G. Zhang, D. Carloni, Y. Wu, *Ceram. Int.* **46**, 21757–21761 (2020)
7. Y. Lv, J. Ma, W. Mi, C. Luan, Z. Zhu, H. Xiao, *Vacuum* **86**, 1850–1854 (2012)
8. X. Yang, X. Du, L. He, D. Wang, C. Zhao, J. Liu, J. Ma, H. Xiao, *J. Mater. Sci.* **55**, 8231–8240 (2020)
9. P. Wellenius, A. Suresh, J.V. Foreman, H.O. Everitt, J.M. Muth, *Mat. Sci. Eng. B-Adv.* **146**, 252–255 (2008)
10. Z. Chen, X. Wang, F. Zhang, S. Noda, K. Saito, T. Tanaka, M. Nishio, M. Arita, Q. Guo, *Appl. Phys. Lett.* **109**, 022107 (2016)
11. Z. Chen, D. Guo, P. Li, Z. Chen, W. Tang, Q. Guo, *Appl. Phys. Exp.* **12**, 061009 (2019)
12. W. Guo, J. Tai, J. Liu, J. Sun, *J. Electron. Mater.* **48**, 5195–5201 (2019)
13. G. Zhang, X. Guo, F. Ren, Y. Li, B. Liu, J. Ye, H. Ge, Z. Xie, R. Zhang, H. Tan, C. Jagadish, *ACS Photonics* **3**, 1912–1918 (2016)
14. X. Yang, X. Du, J. Liu, R. Chen, D. Wang, Y. Le, H. Zhu, B. Feng, J. Ma, H. Xiao, *Ceram. Int.* **47**, 9597–9605 (2021)

15. S.R. Yousefi, M. Masjedi-Arani, M.S. Morassaei, M. Salavati-Niasari, H. Moayedi, *Int. J. Hydrogen Energy* **44**, 24005–24016 (2019)
16. S.R. Yousefi, O. Amiri, M. Salavati-Niasari, *Ultrason. Sonochem* **58**, 104619 (2019)
17. S.R. Yousefi, H.A. Alshamsi, O. Amiri, M. Salavati-Niasari, *J. Mol. Liq.* **337**, 116405 (2021)
18. M.A. Mahdi, S.R. Yousefi, L.S. Jasim, M. Salavati-Niasari, *Int. J. Hydrogen Energy* **47**, 14319–14330 (2022)
19. S.R. Yousefi, A. Sobhani, M. Salavati-Niasari, *Adv. Powder Technol.* **28**, 1258–1262 (2017)
20. S.R. Yousefi, D. Ghanbari, M. Salavati-Niasari, *J. Nanostruct.* **6**, 77–82 (2016)
21. S.R. Yousefi, M. Ghanbari, OAmiriZ. Marzhoseyni, P. Mehdizadeh, M. Hajizadeh-Oghaz, M. Salavati-Niasari, *J. Am. Ceram. Soc.* **104**, 2952–2965 (2021)
22. S.R. Yousefi, A. Sobhani, H.A. Alshamsic, M. Salavati-Niasari, *RSC Adv.* **11**, 11500 (2021)
23. C. Zhao, X. Yang, B. Wei, J. Liu, R. Chen, C. Luan, H. Xiao, *Vacuum* **182**, 109669 (2020)
24. Y. Le, X. Ma, D. Wang, H. Xiao, C. Luan, B. Zhang, J. Ma, *Ceram. Int.* **48**, 26800–26805 (2022)
25. D. Wang, L. He, Y. Le, X. Feng, C. Luan, H. Xiao, J. Ma, *Ceram. Int.* **46**, 4568–4572 (2022)
26. D.D. Hile, H.C. Swart, S.V. Motloung, R.E. Kroon, K.O. Egbo, L.F. Koao, *J. Phys. Chem. Sol.* **140**, 10938 (2020)
27. B. Zhang, C. Luan, D. Wang, H. Xiao, X. Feng, Y. Le, J. Ma, *Ceram. Int.* **48**, 4312–4317 (2022)
28. Y. Le, C. Luan, D. Wang, B. Zhang, H. Xiao, J. Ma, *Mater. Lett.* **302**, 130395 (2021)
29. S. Kumari, S. Chuhadiya, D. Suthar, M.D. Himanshu, N. Kannan, M.S. Kumari, Dhaka, *J. Mater. Sci.* **57**, 19466–19489 (2022)
30. D. Suthar, S.L. Himanshu, S. Patel, M.D. Chander, M.S. Kannan, Dhaka, *J. Mater. Sci.: Mater. Electron.* **32**, 19070–19082 (2021)
31. G. Chasta, S.L. Himanshu, S. Patel, M.D. Chander, M.S. Kannan, Dhaka, *J. Mater. Sci.: Mater. Electron.* **33**, 139–157 (2022)
32. L. He, C. Luan, X. Feng, H. Xiao, X. Yang, D. Wang, J. Ma, *Mater. Res. Bull.* **118**, 110488 (2019)
33. Y. Kajita, H. Nishinaka, M. Yoshimoto, *CrystEngComm* **24**, 3239–3245 (2022)
34. G. Greczynski, L. Hultman, *Sci. Rep.* **11**, 11195 (2021)
35. M. Yadav, A. Mondal, S. Das, S. Sharma, A. Bag, *J. Alloy Compd.* **819**, 153052 (2020)
36. A. Petitmangin, B. Gallas, C. Hebert, J. Perrière, L. Binet, P. Barboux, X. Portier, *Appl. Surf. Sci.* **278**, 153–157 (2013)
37. M. Tadjer, M. Mastro, N. Mahadik, M. Currie, V. Wheeler, J. Freitas, J. Greenlee, J. Hite, K. Hobart, C. Eddy, F. Kub, *J. Electron. Mater.* **45**, 2031–2037 (2016)
38. W. Mi, J. Ma, C. Luan, Y. Lv, H. Xiao, Z. Li, *Mater. Lett.* **87**, 109–112 (2012)
39. H. Yang, Y. Qian, C. Zhang, D.-S. Wu, D.N. Talwar, H.-H. Lin, J.-F. Lee, L. Wan, K. He, Z. Feng, *Appl. Surf. Sci.* **479**, 1246–1253 (2019)
40. X. Liu, K. Li, X. Sun, Z. Shi, Z. Huang, Z. Li, L. Min, V. Botcha, X. Chen, X. Xu, D. Li, *J. Alloy Compd.* **793**, 599–603 (2019)
41. S. Khartsev, N. Nordell, M. Hammar, J. Purans, A. Hallén, *Phys. Status Solidi B* **258**, 2000362 (2021)
42. Y. An, L. Dai, Y. Wu, B. Wu, Y. Zhao, T. Liu, H. Hao, Z. Li, G. Niu, J. Zhang, Z. Quan, S. Ding, *J. Adv. Dielect.* **9**, 1950032 (2019)
43. J. Wang, Z. Wang, B. Huang, Y. Ma, Y. Liu, X. Qin, X. Zhang, Y. Dai, *ACS Appl. Mater. Interfaces* **4**, 4024–4030 (2012)
44. L. Dong, R. Jia, B. Xin, B. Peng, Y. Zhang, *Sci. Rep.* **7**, 1–12 (2017)
45. M. Yu, J. Lin, Z. Wang, J. Fu, S. Wang, H.J. Zhang, Y.C. Han, *Chem. Mater.* **14**, 2224–2231 (2002)
46. Z. Chen, K. Saito, T. Tanaka, Q. Guo, *CrystEngComm* **19**, 4448–4458 (2017)
47. L. Dong, R. Jia, C. Li, B. Xin, Y. Zhang, *J. Alloy Compd.* **712**, 379–385 (2017)
48. L. Dong, P. Li, Y. Zhao, Y. Miao, B. Peng, B. Xin, W. Liu, *Appl. Surf. Sci.* **602**, 154382 (2022)

**Publisher's Note** Springer Nature remains neutral with regard to jurisdictional claims in published maps and institutional affiliations.

Springer Nature or its licensor (e.g. a society or other partner) holds exclusive rights to this article under a publishing agreement with the author(s) or other rightsholder(s); author self-archiving of the accepted manuscript version of this article is solely governed by the terms of such publishing agreement and applicable law.